DECREASING THE LHC IMPEDANCE WITH A NONLINEAR COLLIMATION SYSTEM

J. Resta-López[1,2], A. Faus-Golfe[1], D. Schulte[2] and F. Zimmermann[2]
[1] *IFIC, Valencia, Spain*
[2] *CERN, Geneva, Switzerland*

Abstract

A two-stage nonlinear collimation system based on a pair of skew sextupoles is presented for the LHC. We show the details of the optics design and study the halo cleaning efficiency of such a system. This nonlinear collimation system would allow opening up collimator gaps, and thereby reduce the collimator impedance, which presently limits the LHC beam intensity. Assuming the nominal LHC beam at 7 TeV, the transverse coherent tune shifts of rigid-dipole coupled-bunch modes are computed for both the baseline linear collimation system and the proposed nonlinear one. In either case, the tune shifts of the most unstable modes are compared with the stability diagrams for Landau damping.

INTRODUCTION

A collimation system for the LHC should (i) prevent beam-loss induced quenches of the superconducting LHC magnets; (ii) minimize activation of accelerator components outside of the dedicated collimation insertions; (iii) ensure an acceptable background in the particle-physics experiments; (iv) withstand the impact of eight bunches in case of an irregular beam dump; and (v) not introduce intolerable wake fields that might compromise beam stability [1]. Larger aperture of the mechanical collimators is desired in order to avoid unacceptable high transverse resistive impedance from the collimators and to fulfil the above requirements. We propose a nonlinear collimation system for 7 TeV LHC as a possible solution to this difficult trade-off between cleaning efficiency, collimator robustness and collimator impedance. Earlier studies of nonlinear collimation systems have been described in the literature for linear colliders [2, 3, 4, 5, 6]:

- For the NLC, in Ref. [2] a scheme with skew-sextupole pairs for nonlinear collimation in the vertical plane was proposed.
- Subsequently, in Ref. [3] a halo reduction method with the addition of "tail-folding" octupoles ('Chebyshev arrangement of octupoles') in the NLC final focus system was presented (see also [4] for an earlier study with only 1 octupole in front of the final doublet).
- For the TESLA post-linac collimation system a magnetic energy spoiler (MES) was suggested [5]. A octupole is placed at a high dispersion point between a pair of skew sextupoles (at $\pi/2$ phase advance from the octupole). The skew sextupoles are separated by a optical transfer matrix $-I$. The result is a significant increase in the vertical beam size at a downstream momentum spoiler.

A characteristic feature of all these systems is that they separate between energy and betatron collimation, and typically employ the nonlinear elements only in one or the other half.

A nonlinear collimation system for CLIC with a pair of skew sextupoles was explored [6]. It presents a single vertical spoiler which collimates in the transversal betatron degrees of freedom and in energy. This solution tended to introduce large chromaticity, difficult to correct locally. Recently, a nonlinear design for collimation only in energy was presented as a protection system for CLIC [7]. The scheme is illustrated in Fig. 1. The purpose of the first skew sextupole is to blow up beam sizes and particles amplitudes, so that, on one hand, the transverse beam energy density can be reduced at spoiler position and, on the other hand, the spoiler jaws can be placed further away from the nominal beam orbit. A skew sextupole downstream of the spoiler, and π phase advance from the first sextupole, cancels the geometric aberrations induced by the former.

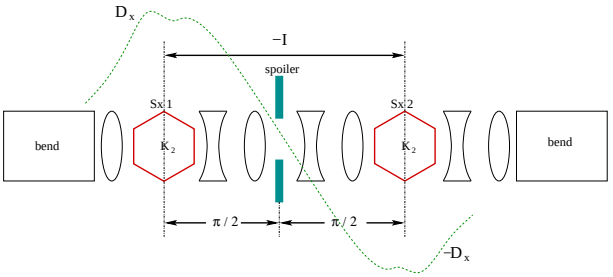

Figure 1: Schematic of a nonlinear collimation system using a pair of skew sextupoles and a single spoiler for CLIC.

For linear colliders designed to operate at center-of-mass energy $\sim$ TeV, the collimation requirements are similar to those for the LHC. It is thus a close thought to apply a similar nonlinear collimation scheme as that designed for CLIC. The main differences from CLIC are the following:

- the LHC momentum spread is almost two orders of magnitude smaller, and, hence, cannot be exploited for widening the beam during collimation;
- emittance growth from synchrotron radiation is insignificant, and does not constrain the design of the collimation system;
- the geometric vertical emittance is about 3 orders of magnitude larger than in CLIC.

In this paper we will present first the present status of the nonlinear betatron cleaning insertion for the LHC. We will present the optics solution and a nonlinear two-stage collimation system, i.e. including primary and secondary collimators. Results of its performance and cleaning efficiency from simulation studies will be shown.

Finally, the impedance of the proposed design will be study and compared with those of the conventional baseline linear collimation system of Phase-I [8, 9].

OPTICS LAYOUT

In this section we discuss the optical constraints for a system based on a skew sextupoles pair as shown in the schematic of Figure 6, which represents the interaction region IR7 of the LHC adapted for nonlinear betatronic collimation. In this lattice, the spoiler or primary collimator is placed at (or near) the interaction point IP7.

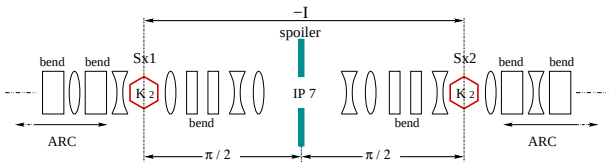

Figure 2: Schematic of a nonlinear collimation layout for the LHC.

The beam motion in a skew sextupole at a location with horizontal dispersion $D_{x,\mathrm{s}}$ is given by the Hamiltonian

$$H_s = \frac{1}{6}K_s(y_{\beta,\mathrm{s}}^3 - 3(x_{\beta,\mathrm{s}} + D_{x,\mathrm{s}}\delta)^2 y_{\beta,\mathrm{s}}) \ , \qquad (1)$$

where $x_{\beta,\mathrm{s}}$ and $y_{\beta,\mathrm{s}}$ are the transverse betatron amplitudes at the sextupole, and δ the relative momentum offset. We assume no dispersion in the vertical plane. The integrated sextupole strength K_s can be expressed in terms of the sextupole length l_s, the pole-tip field B_T, the magnetic rigidity $B\rho$ and the sextupole aperture a_s as $K_s = 2B_T l_s/(B\rho)a_s^2$.

At the sextupole a charged particle suffers the following deflections:

$$\begin{aligned} \Delta x' &= -\frac{\partial H_s}{\partial x_{\beta,\mathrm{s}}} \\ &\simeq K_s x_{\beta,\mathrm{s}} y_{\beta,\mathrm{s}} \ , \qquad (2) \\ \Delta y' &= -\frac{\partial H_s}{\partial y_{\beta,\mathrm{s}}} \\ &\simeq -\frac{1}{2}K_s(y_{\beta,\mathrm{s}}^2 - x_{\beta,\mathrm{s}}^2) \ . \qquad (3) \end{aligned}$$

Here in the second step the dispersive term $D_{x,\mathrm{s}}\delta$ have been neglected. We have assumed $D_{x,\mathrm{s}}\delta$ much smaller than the betatron amplitudes x_β and y_β both at the sextupole and at the spoiler.

The transverse position at the downstream spoiler is obtained from

$$\begin{aligned} x_{\mathrm{sp}} &= x_{0,\mathrm{sp}} + R_{12}\Delta x' \ , \qquad (4) \\ y_{\mathrm{sp}} &= y_{0,\mathrm{sp}} + R_{34}\Delta y' \ , \qquad (5) \end{aligned}$$

where $x_{0,\mathrm{sp}} = x_{\beta,\mathrm{sp}} + D_{x,\mathrm{sp}}\delta \simeq x_{\beta,\mathrm{sp}}$ and $y_{0,\mathrm{sp}} = y_{\beta,\mathrm{sp}}$ are the horizontal and vertical position of the particle at the spoiler without the sextupole, written in terms of the betatronic parts, $x_{\beta,\mathrm{sp}}$ and $y_{\beta,\mathrm{sp}}$, and the horizontal dispersion at the spoiler, $D_{x,\mathrm{sp}}$. R_{12} and R_{34} denote the lineal optical transport matrix elements between the skew sextupole and the spoiler.

The root mean squared (rms) transverse beam sizes at the spoiler are given by the following expressions:

$$\begin{aligned} \sigma_{x,\mathrm{sp}} &= \sqrt{\langle x_{\mathrm{sp}}^2\rangle - \langle x_{\mathrm{sp}}\rangle^2} \\ &\simeq \left[K_s^2 R_{12}^2 \beta_{x,\mathrm{s}}\beta_{y,\mathrm{s}}\epsilon_x\epsilon_y + \beta_{x,\mathrm{sp}}\epsilon_x\right]^{1/2} \ , \qquad (6) \\ \sigma_{y,\mathrm{sp}} &= \sqrt{\langle y_{\mathrm{sp}}^2\rangle - \langle y_{\mathrm{sp}}\rangle^2} \\ &\simeq \left[\frac{1}{2}K_s^2 R_{34}^2\left(\beta_{x,\mathrm{s}}^2\epsilon_x^2 + \beta_{y,\mathrm{s}}^2\epsilon_y^2\right) + \beta_{y,\mathrm{sp}}\epsilon_y\right]^{1/2} \qquad (7) \end{aligned}$$

Collimation depth and collimator apertures

Let $\pm n_x\sqrt{\beta_{x,\mathrm{s}}\epsilon_x}$ and $\pm n_y\sqrt{\beta_{y,\mathrm{s}}\epsilon_y}$ be the collimation amplitudes for the horizontal and vertical betatron motion respectively, and $\pm n_{x2}\sqrt{\beta_{x,\mathrm{sp}}\epsilon_x}$ and $\pm n_{y2}\sqrt{\beta_{y,\mathrm{sp}}\epsilon_y}$ the physical transverse apertures of the primary spoiler. Then for the collimation to function in either transverse plane, we must have the following vertical spoiler half gap:

$$\begin{aligned} a_y \equiv n_{y2}\sqrt{\beta_{y,\mathrm{sp}}\epsilon_y} &= \frac{1}{2}K_s R_{34} n_x^2 \beta_{x,\mathrm{s}}\epsilon_x \ , \qquad (8) \\ a_y \equiv n_{y2}\sqrt{\beta_{y,\mathrm{sp}}\epsilon_y} &= \frac{1}{2}K_s R_{34} n_y^2 \beta_{y,\mathrm{s}}\epsilon_y \ . \qquad (9) \end{aligned}$$

This means that particles at transverse amplitudes $|x_\beta| \gtrsim n_x\sqrt{\beta_{x,\mathrm{s}}\epsilon_x}$ and $|y_\beta| \gtrsim n_y\sqrt{\beta_{y,\mathrm{s}}\epsilon_y}$ will be deflected by the first skew sextupole and caught by a vertical spoiler of normalized half gap n_{y2}. On the other hand, particles distributed in a radial plane $|x_\beta| \approx |y_\beta|$ will not be collimated by the vertical spoiler. Instead these particles will receive a horizontal kick by the skew sextupole and can be caught setting the mechanical jaws with the following horizontal half gap:

$$a_x \equiv n_{x2}\sqrt{\beta_{x,\mathrm{sp}}\epsilon_x} = K_s R_{12} n_x n_y \sqrt{\beta_{x,\mathrm{s}}\epsilon_y}\sqrt{\beta_{y,\mathrm{s}}\epsilon_y} \ . \qquad (10)$$

The normalized aperture at the spoiler n_{x2} can be adjusted to improve the cleaning efficiency for particles with offsets in both transverse planes.

In order to approximate a circular collimation aperture in the normalized x–y plane we can choose $\beta_{x,s} = \beta_{y,s}$ at the skew sextupoles and $R_{12} \simeq R_{34}$. In this case, from the system of Eqs. (8), (9) and (10), we have $n_{x2} = 2n_{y2}$.

Taking into account that the collimation depth for the LHC is established at $n_x = n_y = 6$ [8], we have looked for optics solutions that allow the setting of the vertical and horizontal spoiler jaws with half gaps $n_{y2} = 8$ and $n_{x2} = 2n_{y2} = 16$, respectively.

Spoiler protection

An important function of the collimator system is the protection of the spoiler against beam impacts which may possibly damage it. Considering gaussian beams, a minimum transverse beam size $\sigma_{r,\min}$ is required for spoiler survival in case of full beam impact, and then the beam area at the spoiler must satisfy

$$\sigma_{x,\mathrm{sp}}\sigma_{y,\mathrm{sp}} \gtrsim \sigma^2_{r,\min} \ . \tag{11}$$

In the case of the LHC, primary collimators (made of graphite) a minimum rms beam size $\sigma_{r,\min}$ of about 200 μm has been estimated [10].

The above condition can be rewrite using the Eqs. (6) and (7), with $\beta_{x,\mathrm{s}} = \beta_{y,\mathrm{s}}$ and $\epsilon_x = \epsilon_y \equiv \epsilon$, as

$$(K_s^2 R_{12}^2 \beta_{x,\mathrm{s}}^2 \epsilon + \beta_{x,\mathrm{sp}})(K_s^2 R_{34}^2 \beta_{x,\mathrm{s}}^2 \epsilon + \beta_{y,\mathrm{sp}})\epsilon^2 \gtrsim \sigma^4_{r,\min} \ . \tag{12}$$

From Eq. (10) we can obtain

$$\beta_{x,\mathrm{s}} = \left(\frac{n_{x2}^2 \beta_{x,\mathrm{sp}}}{K_s^2 R_{12}^2 n_x^4 \epsilon} \right)^{1/2} \ . \tag{13}$$

Combining Eq. (12) and Eq. (13), one obtains the spoiler survival condition in terms of the collimation depth n_x and of the collimator aperture n_{x2}, i.e.

$$\left(\frac{n_{x2}^2}{n_x^4} + 1 \right) \left(\frac{\beta_{y,\mathrm{sp}}}{\beta_{x,\mathrm{sp}}} + \frac{R_{34}^2 n_{x2}^2}{R_{12}^2 n_x^4} \right) \beta_{x,\mathrm{sp}}^2 \epsilon^2 \gtrsim \sigma^4_{r,\min} \ , \tag{14}$$

This condition constrains approximately the minimum values of K_s, R_{12} and R_{34} permitted. However to establish a more accurate limit to avoid the collimator damage detailed numerical simulations would be necessary. Related to this topic see for example [11, 12].

Optics solution

The optics for the betatronic cleaning insertion IR7 in LHC optics version 6.5 has been matched to fulfil the previous nonlinear collimation requirements, minimizing both the sextupole strength and the product of sextupole strength and beta function at the sextupole in order to reduce as much as possible the nonlinear aberrations. The matching was done without affecting the optics of the other LHC insertions, and involved only existing quadrupole magnets. Table 1 summarizes the main parameters of the choosen optics solution. Figure 3 shows the betatron functions and dispersion of this optics solution as function of the longitudinal coordinate s.

Table 1: Optics parameters for a nonlinear collimation section in IR7 of LHC.

variable	value
beta functions (x, y) at skew sext.	200.0, 200.0 m
product of skew sextupole pole-tip field and length $(B_T l_s)$	8.1823 T·m
skew sextupole aperture a_s	10 mm
skew sextupole strength K_s	7.0063 m^{-2}
R_{12}, R_{34} from sext. to spoiler	124.403, 124.404 m
beta functions (x, y) at spoiler	77.381, 77.381 m
rms spot size (x, y) at spoiler	215.89, 263.96 μm

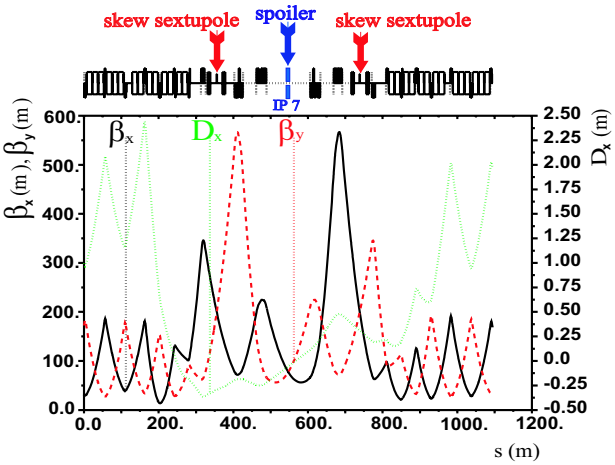

Figure 3: Betatron functions and dispersion versus s for LHC IR7 with a nonlinear section based on two skew sextupoles.

In the particular case of our optics solution, where $\beta_{y,\mathrm{sp}} = \beta_{x,\mathrm{sp}}$ and $R_{34} \simeq R_{12}$, one can rewrite Eq. (14) as

$$\left(\frac{n_{x2}^2}{n_x^4} + 1 \right)^2 \beta_{x,\mathrm{sp}}^2 \epsilon^2 \gtrsim \sigma^4_{r,\min} \ . \tag{15}$$

Collimation boundaries

From the collimator apertures $n_{x2} = 16$ and $n_{y2} = 8$ and using the optics parameters of Table 1, we can compute the collimation contours, given by the equations:

$$n_{x2} = \frac{\beta_{x,\mathrm{s}}\epsilon}{\sqrt{\beta_{x,\mathrm{sp}}\epsilon}} R_{12} K_s \widetilde{n}_x \widetilde{n}_y \ , \tag{16}$$

$$n_{y2} = \frac{\beta_{x,\mathrm{s}}\epsilon}{\sqrt{\beta_{x,\mathrm{sp}}\epsilon}} \frac{1}{2} R_{34} K_s (\widetilde{n}_x^2 - \widetilde{n}_y^2) \ , \tag{17}$$

expressed in normalized coordinates (in units of $\widetilde{n}_x = x/\sqrt{\beta_x \epsilon_x}$ and $\widetilde{n}_y = y/\sqrt{\beta_y \epsilon_y}$).

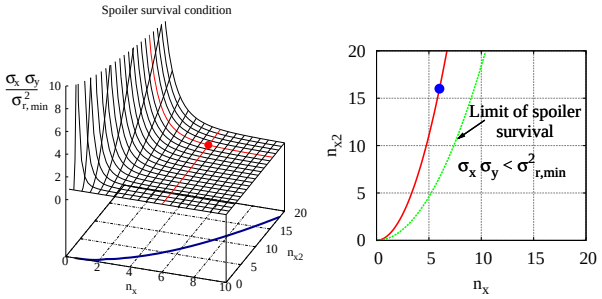

Figure 4: Left: surface $\sigma_x\sigma_y/\sigma^2_{r,\min}$ as function of n_x and n_{x2}. The point represents the working point $n_x = 6, n_{x2} = 2n_{y2} = 16$ and $\sigma_x\sigma_y/\sigma^2_{r,\min} = 1.158$. The solid line in the plane n_{x2} vs. n_x represents the limit $\sigma_x\sigma_y/\sigma^2_{r,\min} = 1$ for spoiler survival when $n_{x2} = 2n_{y2}$. Right: mechanical spoiler aperture vs. collimation amplitude. The red line is the relation n_{x2} vs. n_x as given by Eq. (8). The green line represents the limit $\sigma_x\sigma_y/\sigma^2_{r,\min} = 1$ for spoiler survival.

Figure 5 shows the resulting collimation boundaries. Particles incoming to the sextupole with amplitude offsets $\gtrsim 6\sigma$ will be kicked and, in the ideal case, lost in the downstream collimators. Note that the boundaries here shown refer to vanishing initial slopes, and they would be modified for trayectories with initial x' or y' unequal zero.

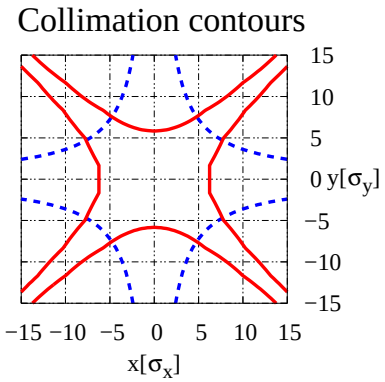

Figure 5: Collimation boundaries for $x' = y' = 0$, with $n_{y2} = 8$ and $n_{x2} = 2n_{y2}$.

TWO-STAGE COLLIMATION

Until now we have only considered spoilers or primary collimators located at IP7. However, protons which are not absorbed can be scattered elastically off the jaw, thus generating a secondary halo which can induce quenches of the superconducting magnets. Therefore, secondary collimators are necessary to intercept the secondary halo. The gaps of the existing collimators in the IR7 insertion of the LHC [9] were set to the required apertures for nonlinear collimation. A total of 12 secondary collimators are retained downstream the primary collimators. Notably a vertical collimator is located at the optimum phase advance $\Delta\mu_0 \simeq 0.476$ rad from IP7, calculated from $\Delta\mu_0 = \pm\arccos(n_{y2}/n'_{y2})$ [13], assuming a primary vertical aperture $n_{y2} = 8$ and a secondary vertical aperture $n'_{y2} = 9$. The other possible solutions $\Delta\mu_0 = 0.476 + \pi$ rad and $\Delta\mu_0 = \pi - 0.476$ have been rejected, since at these phase advances one is in the arc downstream the collimation region, where superconducting dipoles are placed.

The data of the location of the secondary collimators for the nonlinear system are given in Table 2. Secondary collimators between IP7 and the second skew sextupole have been set with a radial aperture of 9σ, and those downstream of the second skew sextupole with 7σ. See the schematic of Figure 6.

Figure 7 compares the half gap of the collimators for the linear and the alternative nonlinear collimation systems. The total number of active collimators in IR7 is 14 for the nonlinear system and 19 for the linear system (Phase-I system). The empty space in the histogram of Figure 7 indicates the space reserve for future system upgrades. For the nonlinear collimation system we have added the secondary collimators $\#14$, $\#15$ and $\#17$ using that existing space reserve.

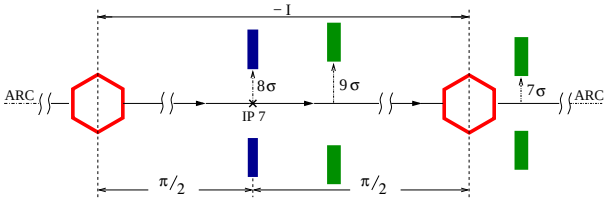

Figure 6: Schematic of a two-stage nonlinear collimation layout for the LHC.

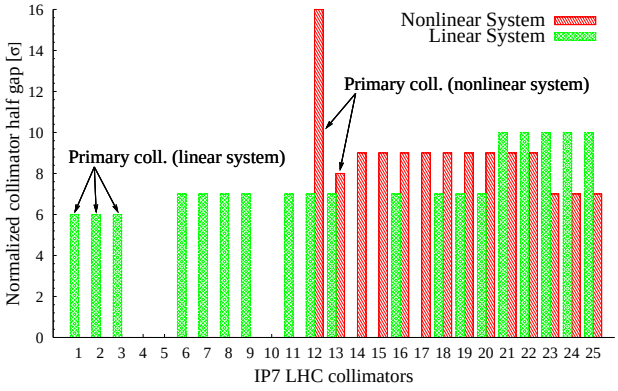

Figure 7: Comparison of the normalized collimator apertures for the nonlinear and the linear collimation systems. In the nonlinear case, the collimators $[\#1, \#11]$ are not used, and collimators $\#12$ with $n_{x2} = 16$ and $\#13$ with $n_{y2} = 8$ play the role of primary spoilers at IP7.

CLEANING EFFICIENCY

Tracking studies have been performed for the nonlinear and linear collimation systems by using a extended version of the tracking code `SixTrack` for collimation studies

Table 2: Data of primary and secondary collimators of the proposed two-stage nonlinear collimation insertion IR7: reference number of order in cleaning insertion, name of the collimator (maintaining the same nomenclature of Phase-I), collimator material, collimator length distance taking IP7 as a reference point, skew angle and half gaps in units of σ. The names with the superindex $^{(*)}$ indicate additional collimators, which are not present in the baseline linear collimation system of Phase-I.

#	Name	Material	Length [m]	Distance from IP7 [m]	Azimuth [rad]	Half gap [σ_β]
Primary						
12	TCSG.A4L7.B1	C	0.6	-3.	0.	16
13	TCSG.A4R7.B1	C	0.6	1.	1.571	8
Secondary						
14	TCSG.B4R7.B1$^{(*)}$	C	1.0	53.190	1.571	9
15	TCSG.A5R7.B1$^{(*)}$	C	1.0	88.256	0.651	9
16	TCSG.B5R7.B1	C	1.0	92.256	2.47	9
17	TCSG.C5R7.B1$^{(*)}$	C	1.0	104.256	1.571	9
18	TCSG.D5R7.B1	C	1.0	108.256	0.897	9
19	TCSG.E5R7.B1	C	1.0	112.256	2.277	9
20	TCSG.6R7.B1	C	1.0	146.861	0.009	9
21	TCLA.A6R7.B1	W	1.0	153.927	1.571	9
22	TCLA.C6R7.B1	W	1.0	184.801	0.	9
23	TCLA.E6R7.B1	W	1.0	218.352	1.571	7
24	TCLA.F6R7.B1	W	1.0	220.351	0.	7
25	TCLA.A7R7.B1	W	1.0	237.698	0.	7

[14, 15]. This tool allows us to calculate the cleaning inefficiency of the collimation system and to save the particles trajectories for an offline analysis of beam losses.

The cleaning inefficiency $\eta_c(A_0)$ of the collimation system is defined by [14]

$$\eta_c(A_0) = \frac{N_p(A > A_0)}{N_{\rm abs}}\,, \qquad (18)$$

with $N_p(A > A_0)$ the number of beam protons with amplitude above A_0 and $N_{\rm abs}$ the total number of absorbed protons in the cleaning insertion.

Beam halos have been generated from a tracking of initial distributions of $N_p \simeq 5 \times 10^6$ protons for 200 turns. At first, initial horizontal and vertical halos were separately considered. The initial horizontal distribution in normalized phase space is an annulus with radii $A_x = \sqrt{X^2 + X'^2} = 6.003$ and $A_y = \sqrt{Y + Y'^2} = 0$ and thickness $\delta\sigma = 0.0015\sigma$. Similarly, for the vertical halo we used $A_x = 0$ and $A_y = 6.003$. In a second step, a square particle distribution with diagonal amplitude $A_r = \sqrt{A_x^2 + A_y^2} = 8.503$ ($A_x = A_y \simeq 6$) has been considered to study the skew halo components.

The resulting $\eta_c(A_0)$ for the nonlinear collimation system compared with the linear one is shown in Figure 8. The nonlinear system presents better cleaning efficiency (lower cleaning inefficiency) for $A_0 \in [6\sigma, 7.4\sigma]$ and $A_0 \in [9.5\sigma, 15\sigma]$ for the vertical halo. In the range $(7.4\sigma, 9.5\sigma)$ the linear system is more efficient by not more than a factor 2 superior to the nonlinear one. However, for a horizontal halo, the inefficiency of the nonlinear system in the range $[7.5\sigma, 15\sigma]$ is higher by approximately a factor 10. In the case of a radial halo, the present nonlinear system is less efficient by a factor 3.

The number of impacts and absorptions at every collimator of the nonlinear and linear systems is displayed in Figure 9 for the vertical halo. Unlike the linear system, that registers the peak of impacts and absorptions at the begining of the insertion, the nonlinear system registers the peak at the collimator $\#13$, located close to the IP7.

DECREASING THE LHC IMPEDANCE

Coherent coupled-bunch tune shifts because of collimator impedances

The main part of the LHC collimators in Phase-I will be made of graphite. This material is a poor conductor (its electrical conductivity compared with the copper conductivity $\sigma_{\rm C} \simeq 1.7 \times 10^{-3}\sigma_{\rm Cu}$). In addition, the collimator jaws in Phase-I will be located close to the beam ($a \sim 6\sigma$). These conditions will contribute to increase the impedance of the machine. Calculations [16, 17] have shown that the achievable nominal LHC beam intensity ($\sim 1.1\times10^{11}$), and therefore the luminosity, will be limited by the impedances introduced by the collimators.

A nonlinear collimation system, allowing higher aperture for the main part of the collimators, could be a cure to the performance limitations associated to the collimator impedances.

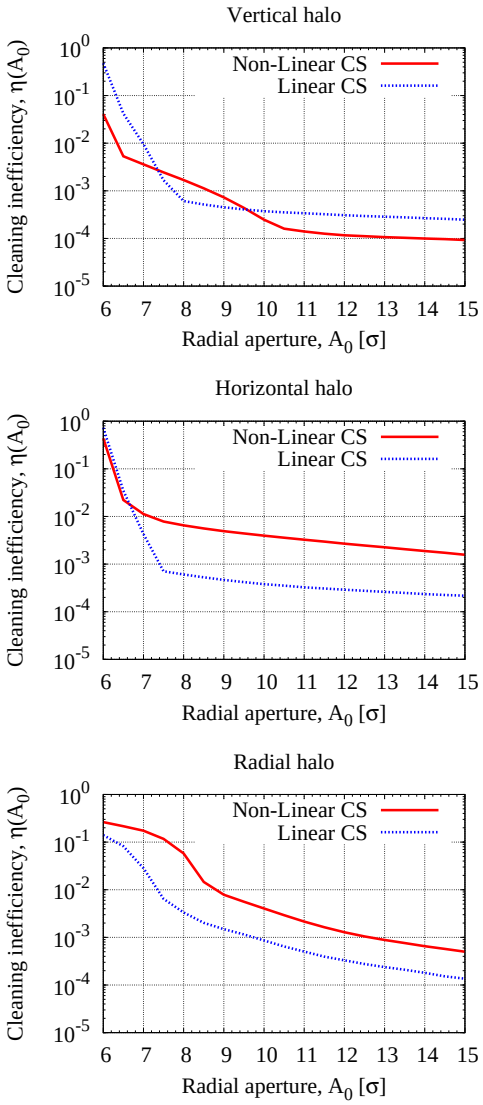

Figure 8: Cleaning inefficiency, $\eta_c(A_0)$, as a function of the radial amplitude A_0 for the nonlinear collimation system (red solid line), compared with $\eta_c(A_0)$ for the conventional linear system (dotted blue line) considering a vertical halo (top), a horizontal halo (middle) and a radial halo (bottom) at 7 TeV.

The calculation of the transverse impedance of each collimator has been performed by using the Burov-Lebedev theory [18, 19]. The contribution from the collimators rotated by an azimuthal angle α have been considered applying the corresponding matrix rotation to a diagonal 2×2 tensor impedance. More details are given in Appendix. The resistive-wall tranverse impedances can generate coherent coupled-bunch tune shift, which can be written in terms of an effective impedance as [20]

$$\Delta Q_\perp(\omega_k - \omega_\xi) = -i \frac{N_\mathrm{b} N e \omega_0 \beta_\perp}{8\pi^2 E} \frac{\Gamma\left(m+\frac{1}{2}\right)}{2^m m!} Z_\perp^{\mathrm{eff}}(\omega_k - \omega_\xi), \quad (19)$$

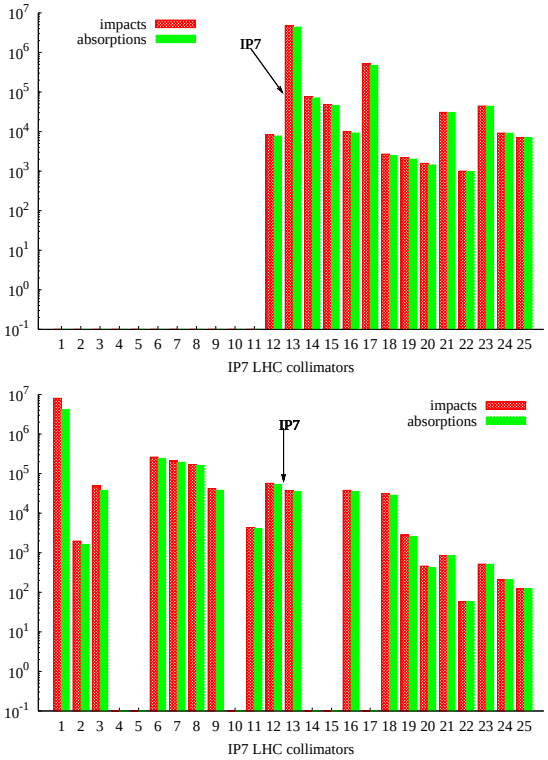

Figure 9: Number of particle impacts and absorptions in the collimators of the insertion IR7 of the LHC for nonlinear collimation (top) and for linear collimation (bottom), if a vertical halo is considered at 7 TeV.

where N is the bunch population, N_b the number of equi-spaced bunches and E the beam energy. It is important to stress the dependence on the frequency $\omega_k = \omega_\beta + k\omega_0 + m\omega_s$, depending of the following oscillation modes: the head-tail mode, characterized by the number m, and the coupled-bunch mode, characterized by the number $l = k - N_\mathrm{b}k'$ with $-\infty \leq k' \leq +\infty$ and $0 \leq l \leq N_\mathrm{b} - 1$. The frequency $\omega_\beta = Q_\beta \omega_0$ denotes the betatron frequency as function of the unperturbed betatron tune Q_β and the revolution frequency of the particles ω_0; ω_s denotes the synchrotron angular frequency and $\omega_\xi = \xi\omega_\beta/\eta$ is the chromatic frequency as function of the chromaticity ξ and the slippage factor η. The expression for the effective impedance can be found in Appendix. By definition the effective impedance measures the degree to which the impedance overlaps the mode spectrum.

We have computed, by using *Mathematica* [21], the total coherent tune shift for both cases, the baseline linear system of Phase-I and the here proposed nonlinear system. On one hand, we added exclusively the contribution of the collimators belonging IR7 insertion (for both cases linear and nonlinear system). On the other hand, we also included the contribution from the total list of collimators, including the insertions IR7, IR3 and the tertiary collimators in IR1, IR2, IR5, IR6 and IR8 for local protection and cleaning at the triplets. Other contributions such as the broad-band (BB) impedance and the resistive wall (RW) impedance without

collimators have also been considered.

In order to select the most unstable case, we have scanned the tune shift versus coupled-bunch modes. The most critical mode is generally that which gives the maximum modules of the tune shifts. Figure 10 shows the module of the horizontal and vertical tunes shifts as a function of the mode number l for the case of the nonlinear IR7. The maxima $|\Delta Q_\perp|$ are found at $l = 0$ and $l = 3564$. The corresponding imaginary part of the tune shift is plotted in Figure 11.

For all calculations we have taken the head-tail mode $m = 0$, related to rigid dipole oscillations, zero chromaticity and the LHC parameters of Table 3. In order to consider a more pesimistic case, we have used $N_\mathrm{b} = 3564$ instead the nominal number of bunches $N_\mathrm{b} = 2808$. Results of $Z_\perp^\mathrm{eff}$ and $\Delta Q_{\perp=x,y}$ are summarized in Table 4 and Table 5, respectively, for each of the different considered contributions.

It is worthwide to point out that when the nonlinear IR7 insertion is used, $|Z_x^\mathrm{eff}|$ is reduced about a factor 2 and $|Z_y^\mathrm{eff}|$ about a factor 3 respect to the linear IR7 insertion of Phase-I.

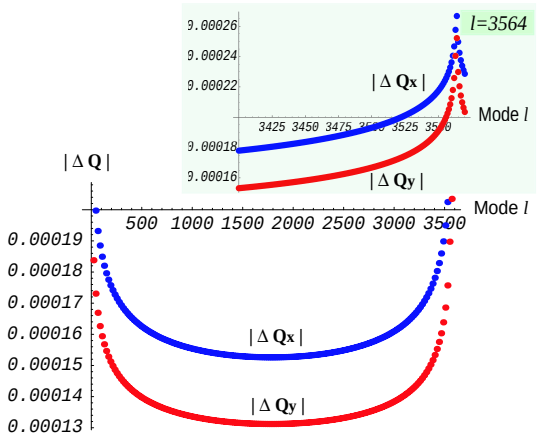

Figure 10: Module of the horizontal ($|\Delta Q_x|$) and the vertical ($|\Delta Q_y|$) coherent coupled-bunch tune shifts as a function of the coupled-bunch mode l for the case of the nonlinear IR7. The figure on the top shows a zoom of the region $l \in [3400, 3575]$. The maxima are found at $l = 0$ and $l = 3564$. The results have been obtained assuming $m = 0$ and $\xi = 0$.

Transverse stability diagrams

Landau damping [22] of the coherent beam oscillation modes provides a possible cure against tune spread instabilities. Because of Landau damping, coherent modes which are present when there is no incoherent tune shift may be absent when such a shift exists. In this way, this can be considered as a bridge between incoherent and coherent beam collective effects.

In the LHC arcs there are two families of magnetic octupoles with the functions of controlling the betatron de-

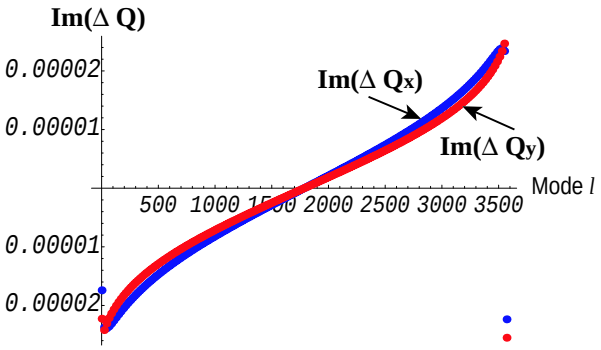

Figure 11: Imaginary part of the horizontal (Im(ΔQ_x)) and the vertical (Im(ΔQ_y)) coherent coupled-bunch tune shift as a function of the coupled-bunch mode l, for the case of the nonlinear IR7. The results have been obtained assuming $m = 0$ and $\xi = 0$.

Table 3: LHC nominal parameters used in the tune shift calculation.

parameter	value
proton energy (at collision): E [TeV]	7.
bunch length: σ_z [mm]	75.5
bunch population: N	1.15×10^{11}
number of bunches: N_b	2808
bunch spacing: Δt_b [ns]	25
revolution frequency: $\omega_0 = 2\pi f_0$ [kHz]	70.6544
betatron tune: Q_β	65.32
machine slippage factor: η	3.22×10^{-4}

tuning with amplitude and providing Landau damping of coherent beam oscillation modes [8]. Potentially unstable oscillation modes with negative imaginary tune shifts would be stabilized by this method.

In order to compare the complex transverse coherent tune shift generated by the collimator impedances from the nonlinear and the linear collimation system, we use the called stability diagrams, introduced first by J. Scott Berg and F. Ruggiero in Ref. [23]. This kind of diagrams represents the limits of the stable beam area in the $-\mathrm{Im}(\Delta Q_\perp)$ versus $\mathrm{Re}(\Delta Q_\perp)$ plane (or equivalently in the $\mathrm{Re}(Z_\perp)$ versus $\mathrm{Im}(Z_\perp)$ plane), granted by the octupole system.

Figure 12 compares the complex tune shift due to the impedances of the nonlinear IR7 and the linear IR7 systems with the Landau damping stability curves, assuming maximum available octupolar strength. The stable area is below the two curves in the figure.

Similarly, Figure 13 compares the tune shifts introduced by the nonlinear and linear IR7 plus the contribution of the IR3 insertion (momentum collimation) and other tertiary collimators in IR1, IR2, IR5, IR6 and IR8 for local protection. The contributions from BB impedance and RW impedance without collimators have also been added.

Table 4: Transverse effective collimator impedance from the IR7 Phase-I (linear), our proposed nonlinear IR7, and other different contributions from: IR3 (momentum collimation insertion), other tertiary collimators for local protection (in IR1, IR2, IR5, IR6 and IR8), broad-band (BB) impedance and resistive wall (RW) impedance without collimators. These results have been obtained considering the most unstable case $m = 0, l = 0$ and $\xi = 0$.

	$Z_x^{\text{eff}}(m=0,l=0,\xi=0)$ [MΩ/m]	$Z_y^{\text{eff}}(m=0,l=0,\xi=0)$ [MΩ/m]
IR7 Phase-I (linear)	$9.309 - 272.321i$	$8.795 - 303.901i$
IR7 (nonlinear)	$9.068 - 120.62i$	$7.084 - 113.64i$
IR3	$1.955 - 38.841i$	$1.089 - 19.917i$
Others (tertiary)	$10.059 - 58.508i$	$9.19 - 47.8i$
RW (w/o collimators)	$41.272 - 8.334i$	$56.994 - 11.508i$
BB (w/o collimators)	$9.237 \times 10^{-6} - 2945.66i$	

Table 5: Transverse coherent coupled-bunch tune shift because of collimator impedance from: IR7 Phase-I (linear), our proposed nonlinear IR7, IR3 (momentum collimation insertion), other tertiary collimators for local protection (in IR1, IR2, IR5, IR6 and IR8), broad-band impedance (BB) and resistive wall (RW) impedance without collimators. These results have been obtained considering the most unstable case $m = 0, l = 0$ and $\xi = 0$.

	$\Delta Q_x(m=0,l=0,\xi=0)$	$\Delta Q_y(m=0,l=0,\xi=0)$
IR7 Phase-I (linear)	$-(6.637 + 0.197i) \times 10^{-4}$	$-(5.127 + 0.146i) \times 10^{-4}$
IR7 (nonlinear)	$-(2.662 + 0.174i) \times 10^{-4}$	$-(2.512 + 0.223i) \times 10^{-4}$
IR3	$-(0.2729 + 0.0217i) \times 10^{-4}$	$-(0.973 + 0.0375i) \times 10^{-4}$
Others (tertiary)	$-(1.259 + 0.222i) \times 10^{-4}$	$-(1.208 + 0.185i) \times 10^{-4}$
RW (w/o collimators)	$-(0.0867 + 0.43i) \times 10^{-4}$	$-(0.12 + 0.593i) \times 10^{-4}$
BB (w/o collimators)	$-(0.438 + 0.i) \times 10^{-4}$	

CONCLUSIONS AND OUTLOOK

We have presented an alternative nonlinear system for betatronic cleaning in the LHC. Its performance and cleaning efficiency have been studied. By adjusting optics and collimator settings, we obtained a considerable improvement of the cleaning efficiency up to the level of the linear system for the vertical direction. However, a careful study is still necessary to further optimize the orientation and positions of secondary collimators to achive the same level of efficiency as the linear system for the cleaning of the horizontal and radial halo components.

A nonlinear collimation system allows larger aperture for the mechanical jaws and thereby reduces the collimator impedance. We have shown how a nonlinear betatronic collimation insertion for the LHC would reduce considerably the coherent tune shift for the most critical coupled-bunch mode as compared with the conventional baseline linear collimation system of Phase-I.

ACKNOWLEDGEMENTS

We would like to thank R. Assmann, S. Redaelli and G. Robert-Demolaize for providing us with the extended version of `SixTrack` for collimation studies and for several helpful discussions and comments.

APPENDIX: COHERENT COUPLED-BUNCH HEAD-TAIL TUNE SHIFT

Burov-Lebedev theory of linear resistive-wall wake field

In [18, 19] Burov and Lebedev (BL) calculated the linear resistive-wall impedance including the effect of the finite chamber thickness. They assumed that the beam wave length is large compared to the beam pipe inner aperture ($c/\omega \gg a$), that the structure is long compared to the aperture ($L \gg a$), and also the relativistic limit $\beta_v \gamma \gg 1$ (here is the relativistic ratio v/c, with v the particle velocity and c the speed of light). From the BL theory for a flat chamber (flat collimator) of thickness d with inner aperture a at an arbitrary transverse plane (1), surrounding by vacuum extending to infinity, the transverse resistive-wall impedance can be approximated by [18]

$$Z_{\perp}^{\text{flat}}(\omega_k) \simeq -i\frac{\pi^2}{12}\frac{Z_0}{2\pi a^2}\frac{1}{1+\tau/2}\ , \qquad (20)$$

with an accuracy better than 5 % for arbitrary $0 \leq \tau \leq \infty$, where $\tau = \kappa a \tanh(\kappa d)$, and $|\kappa|a \gg 1$ is assumed. The value of κ is obtained from

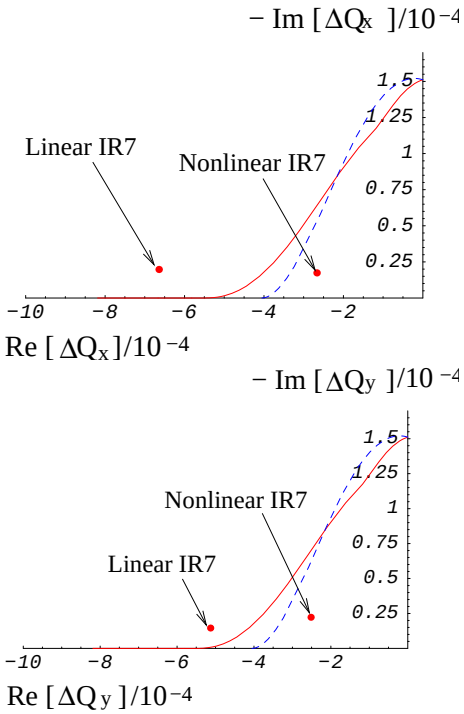

Figure 12: The transverse stability diagram in LHC at 7 TeV, with the nominal bunch population $N = 1.15 \times 10^{11}$ protons. The horizontal and vertical axes represents the real part and minus the imaginary part of the transverse (horizontal on the left and vertical on the right) tune shift, respectively. The points for the nonlinear and linear collimation system are compared. The dashed (blue) curve is the stability for maximum landau octupole current with negative anharmonicity; the slid (red) curve with positive anharmonicity.

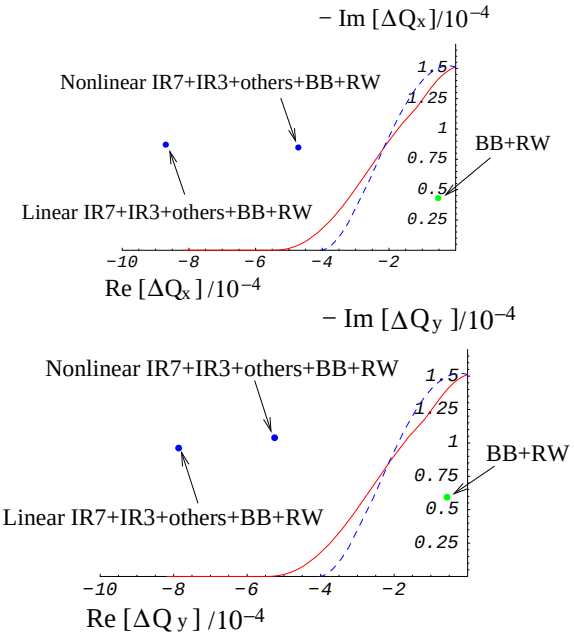

Figure 13: The transverse stability diagram in LHC at 7 TeV, with the nominal bunch population $N = 1.15 \times 10^{11}$ protons. The horizontal and vertical axes represents the real part and minus the imaginary part of the transverse (horizontal on the left and vertical on the right) tune shift, respectively. The points compare the tune shift introduced by the nonlinear and the linear collimation systems, adding the total list of contributions from Table 5. The dashed (blue) curve is the stability for maximum landau octupole current with negative anharmonicity; the slid (red) curve with positive anharmonicity.

$$\kappa = (i + \mathrm{sgn}(\omega_k))\sqrt{\frac{\mu_0 \sigma |\omega_k|}{2}} \ . \qquad (21)$$

The frequency ω_k is given by $\omega_k = \omega_\beta + k\omega_0 + m\omega_s$, with $-\infty \le k \le +\infty$ for a single bunch beam, and $k = l + N_\mathrm{b} k'$ with $-\infty \le k' \le +\infty$ for a multi-bunch beam (such as in the case of the LHC). Here, $\omega_\beta = Q_\beta \omega_0$, with Q_β the unperturbed betatron tune and $\omega_0 = 2\pi f_0$ the average revolution frequency of the particles and $\omega_s = 2\pi f_s$ the synchrotron angular frequency. The number $m = -\infty, \ldots, -1, 0, 1, \ldots, +\infty$ is called the *head-tail mode* number, $l = 0, 1, \ldots, N_\mathrm{b} - 1$ the *coupled-bunch* mode and N_b the number of equi-populated equi-spaced bunches.

The impedance in a plane (2), orthogonal to the plane (1), can be obtained from the Yokoya prescription [24] $Z^{\mathrm{flat}}_{\perp(2)} = (1/2) Z^{\mathrm{flat}}_{\perp(1)}$, i.e.,

$$Z^{\mathrm{flat}}_{\perp(2)} \simeq -i \frac{\pi^2}{24} \frac{Z_0}{2\pi a^2} \frac{1}{1 + \tau/2} \ . \qquad (22)$$

On the other hand, the transverse impedance of a round chamber (round collimator) can be obtained by dividing the expressions (20) and (22) with the factor $\pi^2/12$ and $\pi^2/24$ respectively [24], i.e.,

$$Z^{\mathrm{flat}}_{\perp(1)} = \frac{\pi^2}{12} Z^{\mathrm{round}}_{\perp} \ , \quad Z^{\mathrm{flat}}_{\perp(2)} = \frac{\pi^2}{24} Z^{\mathrm{round}}_{\perp} \ . \qquad (23)$$

Coherent tune shift

Questions such as what modes are more critically excited by the impedance and the the corresponding tune shift of these modes can be more directly addressed using the so-called effective impedance [20, 25], defined as

$$Z^{\mathrm{eff}}_{\perp}(m, l, \xi) \equiv \frac{\sum_{k'=-\infty}^{+\infty} Z_\perp(\omega_{kl}) h_m(\omega_{kl} - \omega_\xi)}{\sum_{k'=-\infty}^{+\infty} h_m(\omega_{kl} - \omega_\xi)} \ , \qquad (24)$$

where the transverse impedance $Z_\perp$ is essentially weighted by the beam power spectrum h_m for a head-tail mode number m. The frequency ω_{kl} is given by $\omega_{kl} = \omega_\beta + (l + N_\mathrm{b} k')\omega_0 + m\omega_s$. The variable $\omega_\xi = \xi \omega_\beta / \eta$ is the trans-

verse chromatic frequency, which is a function of the chromaticity ξ, the betatron frequency ω_β and the slippage factor $\eta = (\Delta T/T_0)(\Delta p/p_0)$, with T and p the revolution period and the momentum of the particle respectively . In the case of a gaussian beam,

$$h_m(\omega) = \left(\frac{\omega\sigma_z}{c}\right)^{2m} e^{-\omega^2\sigma_z^2/c^2} \ . \qquad (25)$$

Figure 14 shows the power spectrum of a gaussian beam for the first three head-tail modes $m = 0, 1$ and 2 depending on the coupled-bunch mode l

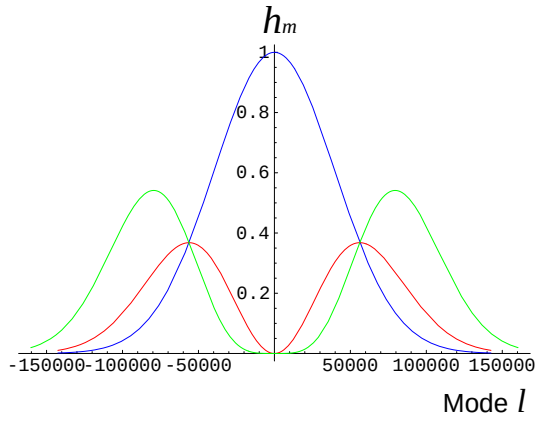

Figure 14: Transverse power spectrum for the first three head-tail modes $m = 0$ (blue), $m = 1$ (red) and $m = 2$ (green), assuming $\xi = 0$ and $p = 0$, versus the coupled-bunch mode number l.

The transverse coherent tune shift becacuse of the collimator impedances can be calculated in terms of the effective impedance (24) by using the following expression [20]:

$$\Delta Q_\perp(m,l,\xi) = -i\frac{N_\mathrm{b}Ne\omega_0\beta_\perp}{8\pi^2E}\frac{\Gamma\left(m+\frac{1}{2}\right)}{2^m m!}Z_\mathrm{eff}(m,l,\xi) \ , \qquad (26)$$

where N is the number of particles per bunch and E the nominal beam energy.

Tilted collimator contribution

The transverse tensor impedance

In order to calculate the impedance contribution from a skew collimator, rotated by an angle α around the longitudinal axis z, we use the tensor impedance [26]

$$\mathbf{Z}_\perp = \mathbf{R}^{-1}\mathbf{Z}'_\perp\mathbf{R} = \begin{pmatrix} Z_x & Z_{xy} \\ Z_{yx} & Z_y \end{pmatrix} \ , \qquad (27)$$

with the following matrix elements:

$$Z_x = Z_{\perp(1)}\cos^2\alpha + Z_{\perp(2)}\sin^2\alpha \ , \qquad (28)$$

$$Z_y = Z_{\perp(2)}\cos^2\alpha + Z_{\perp(1)}\sin^2\alpha \ , \qquad (29)$$

$$Z_{xy} \equiv Z_{yx} = (Z_{\perp(1)} - Z_{\perp(2)})\sin\alpha\cos\alpha \ . \qquad (30)$$

Here, $\mathbf{Z}'_\perp$ is the tensor impedance diagonalized in a frame rotated by angle α around the axis z, i.e.,

$$\mathbf{Z}'_\perp = \begin{pmatrix} Z_{\perp(1)} & 0 \\ 0 & Z_{\perp(2)} \end{pmatrix} \ , \qquad (31)$$

and $\mathbf{R}$ is the usual 2×2 rotation matrix

$$\mathbf{R} = \begin{pmatrix} \cos\alpha & \sin\alpha \\ -\sin\alpha & \cos\alpha \end{pmatrix} \ . \qquad (32)$$

For instance, for a horizontal collimator $(\alpha = 0)$ one has $\mathbf{Z}_\perp(\alpha = 0) = \mathbf{Z}'_\perp$, and for a vertical collimator $Z'_\perp(\alpha = \pi/2) = \mathrm{adj}\{\mathbf{Z}'_\perp\}$.

The tensor tune shift

The corresponding tune shift tensor is given by

$$\Delta\mathbf{Q}_\perp = -i\frac{N_\mathrm{b}Ne\omega_0}{8\pi^2E}\beta_\perp^{1/2}\mathbf{Z}_\perp\beta_\perp^{1/2} \ , \qquad (33)$$

where

$$\beta_\perp = \begin{pmatrix} \beta_x & 0 \\ 0 & \beta_y \end{pmatrix} \qquad (34)$$

defines the diagonal matrix of the betatron functions, β_x and β_y for the horizontal and vertical plane respectively.

If we consider a collimator in an arbitrary plane (1), whose impedance contribution is $Z_{\perp(1)}$, using the same prescription [24] as in Eq. (22), the collimator impedance at the corresponding orthogonal plane (2) can be obtained from the relation $Z_{\perp(2)} = (1/2)Z_{\perp(1)}$. Therefore, one can calculate the transverse coherent tune shift contribution from a collimator rotated an arbitraty angle α using the following expression:

$$\Delta\mathbf{Q}_\perp = \begin{pmatrix} \Delta Q_x & \Delta Q_{xy} \\ \Delta Q_{yx} & \Delta Q_y \end{pmatrix} \ , \qquad (35)$$

with the following matrix elements:

$$\Delta Q_x = -i\frac{N_\mathrm{b}Ne\omega_0}{8\pi^2E}\beta_x(\cos^2\alpha + \frac{1}{2}\sin^2\alpha)\,Z_{\perp(1)} \ , \qquad (36)$$

$$\Delta Q_y = -i\frac{N_\mathrm{b}Ne\omega_0}{8\pi^2E}\beta_y(\frac{1}{2}\cos^2\alpha + \sin^2\alpha)\,Z_{\perp(1)} \ , \qquad (37)$$

$$\Delta Q_{xy} = -i\frac{N_\mathrm{b}Ne\omega_0}{8\pi^2E}\frac{\sqrt{\beta_x\beta_y}}{2}\sin\alpha\cos\alpha\,Z_{\perp(1)} \ . \qquad (38)$$

The non-diagonal element $\Delta Q_{xy} \equiv \Delta Q_{yx}$ corresponds to a coupling term, which would be compensated by the incoherent tune shift [26].

It is worthwhile to notice that in Eqs. (36), (37) and (38) the impedance $Z_{\perp(1)}$ can be replaced by a more general effective impedance for an arbitrary head-tail mode m, adding a normalization factor $\Gamma(m+1/2)/(2^m m!)$, such as in Eqs. (24) and (26).

REFERENCES

[1] R. Assmann et al., "Collimators and Cleaning, Could this Limit the LHC Performance?," LHC Project Workshop-'Chamonix XII' (2003). "Designing and Building a Collimation System for the High-Intensity LHC Beam," PAC2003, Oregon, 2003.

[2] L. Merminga et al., "Collimation systems for a TeV linear collider," Part. Accel. 48, 85 (1994); SLAC-PUB-5165 Rev. May 1994.

[3] R. Brinkmann, P. Raimondi and A. Seryi, "Halo reduction By Means of Non Linear Optical Elements in the NLC Final Focus System," PAC2001, Chicago (2001).

[4] K. Thompson, R. Pitthan, F. Zimmermann, et al., NLC Collimation Meetings, in particular 22.05.98, 29.05.98, and 31.08.98.; see web site: http://www-project.slac.stanford.edu/lc/bdir/meetings_collimation.asp.

[5] R. Brinkmann, N. J. Walker and G. A. Blair, "The TESLA Post-linac Collimation System," DESY TESLA-01-12 (2001).

[6] A. Faus-Golfe and F. Zimmermann, "A Nonlinear Collimation System for CLIC," EPAC2002, Paris, 2002.

[7] A. Faus-Golfe, J. Resta-Lopez and F. Zimmermann, "Nonlinear Collimation in Linear and Circular Colliders," EPAC2006, Edinburgh, 2006.

[8] LHC Design Report, CERN-2004-003 (2004).

[9] R. W. Assmann, "The Final Collimation System for the LHC," EPAC2006, Edinburgh, 2006.

[10] R. W. Assmann, private communication.

[11] V. Vlachoudis, see slides at http://www.cern.ch/lhc-collimation/files/VVlachoudis_06Feb2004.pdf.

[12] J. B. Jeanneret *et al.*, "Beam loss and collimation at LHC," Proceedings of Beam Halo Dynamics Diagnostics, and Collimation, AIP 2003.

[13] J .B. Jeanneret, "Optics of a two-stage collimation system," Phys. Rev. ST Accel. Beams **1** (1998) 081001.

[14] S. Redaelli *et al.*, "LHC Aperture and Commissioning of the Collimation System," Chamonix XIV (2005).

[15] G. Ripken and F. Schmidt, CERN SL 95-12 (AP)(1995) and DESY 95-063 (1995).

[16] J. B. Jeanneret and E. Metral, "Operational constraints in the LHC due to collimation," LHC Project Workshop-'Chamonix XIII' (2004).

[17] E. Metral, R&D and LHC Collective Effects (RLC) Meeting, 21.04.06, see web site: http://ab-abp-rlc.web.cern.ch/ab-abp-rcl/Meetings/2006/2006.04.21/CBI&SBIAtLHCInjection&TopEnergy_RLC_21-04-06.pdf.

[18] A. Burov and V. Lebedev, "Transverse resistive wall impedance for multi-layer flat chambers," EPAC2002, Paris, 2002; FERMILAB-CONF-02-101, June 2002.

[19] A. Burov and V. Lebedev, "Transverse resistive wall impedance for multi-layer round chambers," EPAC2002, Paris, 2002; FERMILAB-CONF-02-100, June 2002.

[20] A. W. Chao, "Physics of Collective Beam Instabilities in High Energy Accelerators," J. Wiley & Sons, Inc, 1993.

[21] S. Wolfram, "Mathematica," Addison-Wesley, 1991.

[22] H. G. Hereward, "Landau Damping," Proceedings of International School of Particle Accelerators, CERN 77-13, p. 219-230, Geneva, 1977; A. Hofmann, "Landau Damping," CERN Accelerator School (CAS), p. 271-304, Zeuthen, Germany, 2003.

[23] J. Scott Berg and F. Ruggiero, "Landau damping with two dimensional betatron tune spread," CERN SL-AP-96-71 (AP), 1996.

[24] K. Yokoya, Part. Acc., **41**, 221 (1993).

[25] F. Sacherer, "Single beam collective phenomena-transverse (bunched beams)," Proceedings of First Course International School on Accelerators, Erice, 1976; Theoretical Aspects of the Behaviour of Beams in Accelerators and Storage Rings, CERN 77-13, p. 210, 1977.

[26] F. Ruggiero, LHC Collective Effects (LCE) Meeting, 03.10.06, see web site: http://ab-abp-rlc.web.cern.ch/ab%2Dabp%2Drlc/Meetings/2003/2003.10.03/TensorImpedanceFR.pdf.